


Spectroscopic evidence of highly correlated electrons in VSe₂T. Yilmaz¹, E. Vescovo¹, J. T. Sadowski² and B. Sinkovic³¹*National Synchrotron Light Source II, Brookhaven National Lab, Upton, New York 11973, USA*²*Center for Functional Nanomaterials, Brookhaven National Lab, Upton, New York 11973, USA*³*Department of Physics, University of Connecticut, Storrs, Connecticut 06269, USA* (Received 19 September 2021; revised 14 March 2022; accepted 1 June 2022; published 10 June 2022)

We present detailed high-resolution angle-resolved photoemission experiments on VSe₂ grown under various conditions. The surface electronic structure optimally grown samples can host high-temperature spectral kink, quasiparticle peak, and the Fermi gap. Collective observation of these electronic features refers to the strong electronic correlation and is usually attributed to the characteristics of superconductors. Temperature evolution of the quasiparticle peak and the Fermi gap also follow the trend observed in high- T_c superconductors as progressive quenching of the quasiparticle peak at a lower temperature than the complete Fermi gap closing. As a result, the quasiparticle peak can be observed up to 100 ± 5 K while the Fermi gap persists up to ~ 150 K. These realizations can guide future studies to induce high-temperature superconductivity in transition metal dichalcogenides as well as understand the physics behind high- T_c superconductors.

DOI: [10.1103/PhysRevB.105.245114](https://doi.org/10.1103/PhysRevB.105.245114)

Layered transition metal dichalcogenides (TMDCs) host an impressive variety of physics, including the Mott insulating state, charge density waves (CDW), and superconductivity [1–4]. This richness offers a possibility to study the interplay between various states of matter. In this manner, tuning the electronic structure of the TMDCs is subject to many studies to drive the transition from one quantum state to another or induce novel electronic states, such as superconductivity in TiSe₂ with Cu doping and negative electronic compressibility in WSe₂ through the surface deposition of alkaline impurities [5,6].

Among TMDCs, 1T-VSe₂ recently regained much attention with multiple CDW states in a monolayer with a wide transition temperature range, and the three-dimensional (3D) CDW transition in the bulk below 110 K with a $4 \times 4 \times 3$ superstructure [7–12]. Recently, magnetoresistance measurements also showed signatures of the Kondo effect in VSe₂ single crystals [13]. Furthermore, monolayer thin films showed no sign of the ferromagnetic order while chemically exfoliated ones hosted room-temperature ferromagnetism [14]. Another interesting observation reported on VSe₂ is that it becomes a superconductor under high pressure with a T_c of 4 K [15]. Evidently, the transport, magnetic, and electronic structure properties of VSe₂ are tunable by the growth method and parameters indicating that further exotic states can be formed.

Here, we report comprehensive high-resolution angle-resolved photoemission (ARPES) experiments of single crystal and thin film VSe₂ samples grown on single-layer graphene (Gr) and highly ordered pyrolytic graphite (HOPG) substrates by molecular beam epitaxy. Our ARPES study reveals that optimally grown 1T-VSe₂ films on HOPG show a high-temperature spectral kink, the quasiparticle peak (QP), and the Fermi gap, simultaneously. Temperature-dependent

photoemission data show that the QP is suppressed at ~ 100 K while the Fermi gap persists at even higher temperatures of up to ~ 150 K. These observations are usually the signature for strongly correlated electrons in a crystal that can give rise to the emergence of the polaronic metal or superconducting states [16,17]. More interestingly, such spectral features and their temperature evolution observed here are the hallmarks of high- T_c superconductors [17–20]. Furthermore, the QP forms a fully gapped circular dispersion in the Fermi surface. This is different from the expected nature of the CDW phase and d -wave superconductivity in which a gap opens at particular momentum points [12,20], but resembles the s -wave superconducting gap [21]. Thereby, our observation can lead to future works regarding superconductivity in TMDCs and establish a connection between TMDCs and other superconductors.

The VSe₂ bulk sample was obtained from the 2*d* semiconductors company with the part number of BLK-VSe₂. Thin films were grown on Gr and HOPG substrates by using molecular beam epitaxy (MBE). The Gr layer was obtained by annealing a SiC substrate at 1500 K for 15 minutes. Both substrates were loaded to the MBE chamber and annealed at 850 K for 30 minutes to clean the surface before deposition. All the thin film samples are 5-ML thick, as estimated by using a quartz thickness monitor with a 15% error bar. Samples were capped with 20-nm amorphous Se film before being removed from the MBE chamber. ARPES experiments and core levels were recorded at the 21-ID-1 ESM beamline of National Synchrotron Light Source II (NSLS-II) with a DA30 Scienta electron spectrometer. The total experimental resolution was better than 15 meV in photoemission. The μ -low energy electron diffraction (μ -LEED) experiments were performed at xX-ray photoemission electron microscopy/low-energy electron microscopy

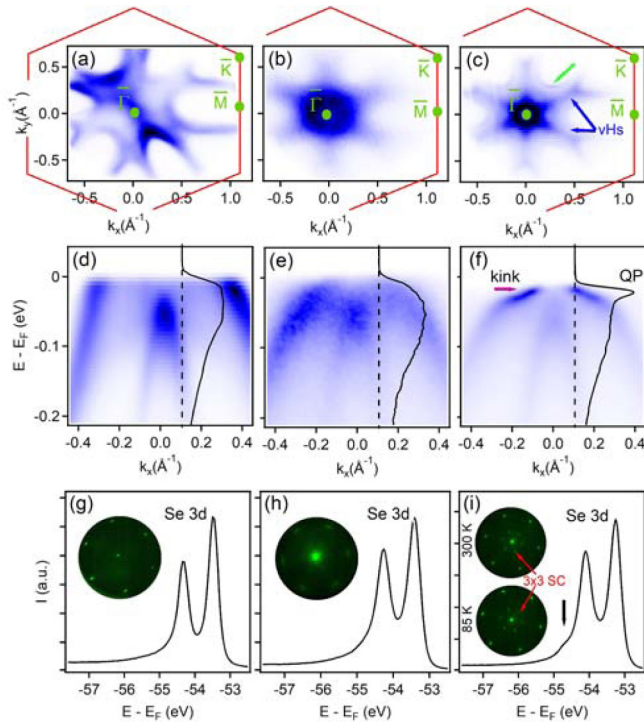


FIG. 1. (a)–(c) Constant energy cuts at 20 meV with respect to the Fermi level obtained from a vacuum cleaved VSe₂ single crystal and VSe₂ thin film on Gr and HOPG, respectively. (d)–(f) Corresponding binding energy versus in-plane momentum (k_{\parallel}) maps taken in the $\bar{\Gamma}$ – \bar{M} direction of the Brillouin zone. Inset figures in (d)–(f) are the EDCs obtained along the dashed black lines. (g)–(i) Corresponding Se 3d peak of each sample recorded with 110 eV photons at 10 K. Inset figures in (g)–(i) are μ -LEED pattern of the corresponding samples. Same growth parameters are adopted for thin films. Red partial hexagons in (a)–(c) represent the Brillouin zone. Blue arrows in (c) show the vHs points while the green arrow marks distinct Fermi arcs from than other two samples. Purple arrow in (f) marks the spectral kink. Black arrow in (i) shows a new spectral feature as a shoulder in the higher binding energy side of Se 3d for the film grown on HOPG. Blue arrow in (f) shows the μ -LEED pattern of Gr. All the ARPES maps are collected with 50-eV photons at 10 K.

(XPEEM/LEEM) end station of the ESM beamline (21-ID-2) at NSLS-II. Before photoemission and diffraction experiments, the VSe₂ samples were annealed at 500 K for 30 minutes under the ultra-high vacuum condition to remove the Se capping layer.

We first compare the electronic and crystal structure of bulk crystal versus thin films as summarized in Fig. 1. The left column is for the bulk single crystal synthesized by the flux zone method. The central and right columns are for two epitaxial films prepared under nominally identical conditions on Gr and HOPG substrates, respectively. At first glance, it is apparent that the qualitative differences distinguish the electronic structure of bulk samples from thin films and, even more surprisingly, also of the two films grown on two similar substrates. The Fermi surface of bulk VSe₂ exhibits two distinct features: an intense emission at the $\bar{\Gamma}$ -point and ellipsoidal electron pockets centered at the \bar{M} -points [Fig. 1(a)].

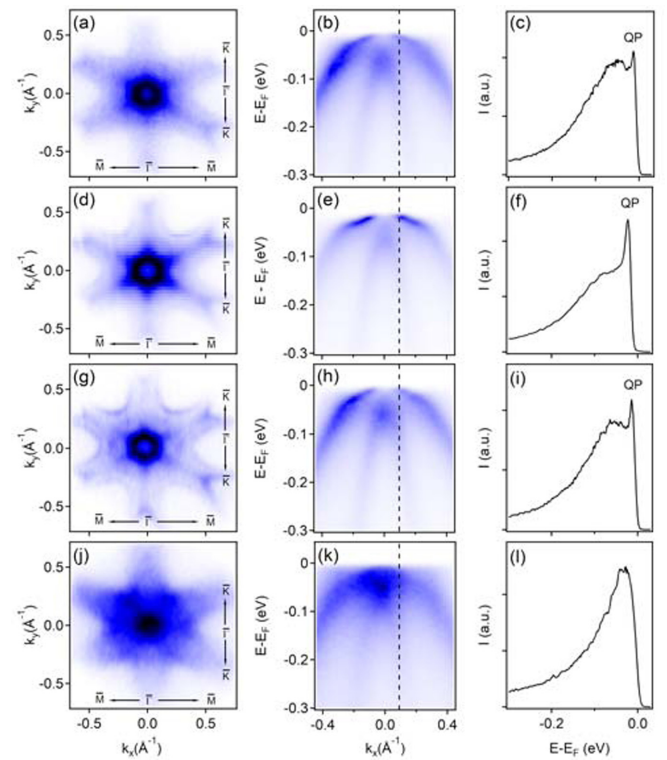


FIG. 2. Left column: Constant energy cuts at 20 meV below the Fermi level. Middle column: ARPES maps along the $\bar{\Gamma}$ – \bar{M} high symmetry direction of the Brillouin zone. Right column: EDCs taken along the dashed line from the corresponding ARPES maps given in middle column. All VSe₂ samples were grown on HOPG in identical conditions except for the substrate temperatures set to 550 K, 570 K, 600 K, and 650 K from top to bottom. Spectra were measured at 10 K with 50-eV photons.

The ellipsoidal features are attributed to the V 3d band, while the emission at the zone center derives from Se 4p atomic orbitals [10]. The energy dispersion of the valence bands along the $\bar{\Gamma}$ – \bar{M} direction is displayed in Fig. 1(d). The V 3d states dominate the region close to the Fermi level while the top of Se 4p reaches the binding energy of about 0.2 eV at the $\bar{\Gamma}$ -point.

Comparing the Fermi surface of the bulk sample to that of the VSe₂ film grown on Gr, the main difference is the formation of a hexagonal-shaped hole pocket centered at the $\bar{\Gamma}$ -point [Fig. 2(b)]. Away from the zone center, the ellipse-shaped electron pockets centered at the \bar{M} -points are similar although less intense than in the bulk sample [Fig. 2(b)]. The binding energy — k_{\parallel} map of the VSe₂ film on Gr exhibits an M-shaped dispersive band in the vicinity of the Fermi level [Fig. 1(e)]. Energy distribution curves (EDCs) of both samples superimposed in Figs. 1(d) and 1(e), respectively, display a similar density of states with a broad bump in the vicinity of the Fermi level. Overall, these results for the single crystal and the thin film grown on Gr are consistent with the literature [8,10].

On the other hand, a VSe₂ film grown on a HOPG substrate shows the most interesting features. New structures develop compared to both the bulk samples and the films on Gr. The center of the Fermi surface assumes a star-like

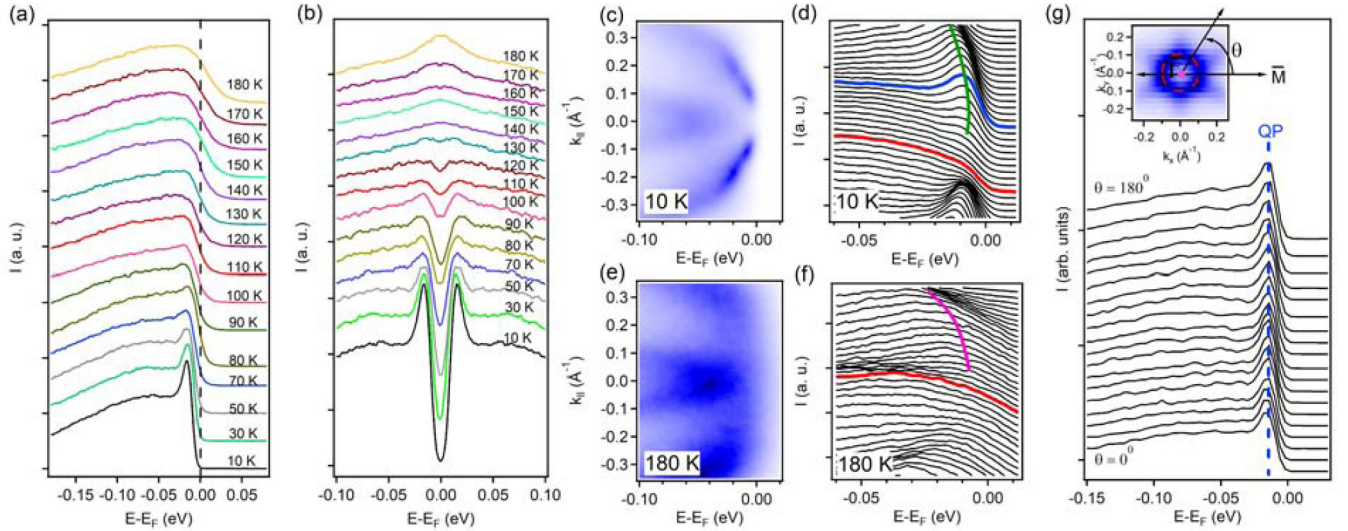


FIG. 3. (a) QP-EDCs vs. temperature. (b) Symmetrized EDCs. (c,d) Dispersion map taken at 10 K and corresponding momentum integrated EDCs. Orange and blue lines in (d) mark the $\bar{\Gamma}$ -point and the Fermi momentum, respectively. Green line in (d) represents the inward band bending. (e) and (f) are the same as (c) and (d) but taken at 180-K sample temperature. Pink line in (f) marks the nearly flat dispersion in the vicinity of the Fermi level and around the $\bar{\Gamma}$ -point. (g) QP-EDCs as a function of the angle- θ given in the inset of (g) measured at 10 K is shown. All the spectra were obtained with 50-eV photons from the sample grown on HOPG substrates at 570-K substrate temperature.

shape and intense triangular pockets centered at the \bar{K} points [Fig. 1(c)]. The vertices of these two features connect along the $\bar{\Gamma}$ - \bar{M} directions at about 1/3 of the way, to form van Hove singularity (vHs) points. The six-fold symmetric ellipsoidal electron pockets centered at the \bar{M} -points are also well resolved in this sample, but are now delimited by extremely sharp momentum arcs [green arrow in Fig. 1(c)]. Also, a circular electron pocket is seen close to the $\bar{\Gamma}$ point [Fig. 1(c)]. These states are concentrated in a narrow energy window of about 25 meV below the Fermi level, possibly resulting from fine-tuning of the chemical potential. Relevant information on the unique electronic structure of this sample is contained in the energy-momentum dispersion map [Fig. 1(f)]. First, the V $3d$ -derived bands approaching the Fermi level exhibit a spectral kink [see purple arrow in Fig. 1(f)]. Second, an intense QP peak is now present in the EDC, followed by a dip and hump of decreasing intensity towards higher binding energy [superimposed in Fig. 1(f)].

To investigate the origin of spectral differences between these samples, we report μ -LEED patterns taken at 300 K and the Se $3d$ peaks for the corresponding samples. The diffraction pattern of single-crystal VSe₂ displays sharp spots, forming the expected three-fold diffraction pattern [inset in Fig. 1(g)]. For the sample grown on the Gr substrate, the diffraction spots are broader and elongated along the tangential direction, indicating the presence of multiple domains [inset in Fig. 1(h)]. The Se $3d$ peaks of both samples show a single doublet line shape, again somewhat broader in the case of the film on Gr [Figs. 1(g) and 1(h)]. Corresponding to the unique features observed in the ARPES data, the μ -LEED pattern for the VSe₂ sample grown on HOPG exhibits a sharp 3×3 superstructure at 300 K and 85 K, unlike the other two samples. Furthermore, the Se $3d$ doublet has an additional component at higher binding energy, marked with a black arrow in Fig. 1(i). These features might indicate the V impurity intercalation which could be responsible for

fine-tuning the chemical potential in the sample grown on HOPG. The low and room temperature μ -LEED data also show that the emergent QP peak, spectral kink, and vHs points in VSe₂ on HOPG cannot be directly associated with periodic distortion in the crystal structure since these spectral features are suppressed at a much lower temperature than 300 K (see Fig. 3 for the temperature evolution of the spectral line in this sample).

Next, we investigate how the growth temperature can further modify the surface electronic structure of VSe₂ films on HOPG. The Fermi surfaces (left column), band dispersions (middle column), and EDCs (right column) demonstrate that the QP, spectral kink, and vHs points are seen in a relatively narrow growth temperature range. At the optimal growth temperature of 570 K, the QP peak exhibits the highest intensity, and the spectral kink is more pronounced [Figs. 2(e) and 2(f)] and both features weaken at lower and higher growth temperatures [Figs. 2(c) and 2(i)]. At the highest growth temperature of 650 K, all these new features disappear [Figs. 2(j) to 2(l)]. This concludes that the new spectral features seen in our work are not only dependent on the sample preparation method and choice of the substrate, but also closely related to the growth parameters.

What is evident from our work is that the surface electronic structure in VSe₂ is tunable by the growth parameters and one can form the QP and spectral kink. These features are usually the signature for strongly correlated electrons which can induce a variety of interesting physics including superconductivity and polarons [16,17]. This refers to the fact that the temperature can play a critical role in its dispersion. Thereby, Fig. 3(a) summarizes the temperature dependence of the QP in the range of 10 K and 180 K. The EDCs measured along the dashed line in Fig. 2(e) show the evolution from a sharp coherent peak at low temperature to a broad incoherent spectral feature at high temperatures. As the temperature increases, the QP weakens but survives up to 100 K. This is quite

a high temperature compared to other materials in the TMDC family and Fe-based bulk superconductors [22]. Specifically, 2H-NbSe₂ shows the QP peak nearly up to 30 K [23]. On the other hand, our observation is comparable to the one seen in cuprate high- T_c superconductors [17].

Except for polaronic metals, the QP and spectral kink usually coexist with a Fermi gap which can be induced by superconductivity or CDW phase. Therefore, to extract and investigate the Fermi gap, symmetrized EDCs are given in Fig. 3(b) where the gap is observed as a spectral dip at the Fermi level. From the symmetrized EDCs, it would appear that the gap persists up to nearly 150 K while the QP is suppressed at lower temperatures. Interestingly, this behavior is identical to high- T_c superconductors, in which a pseudogap can be observed at higher temperatures than the onset temperature of the superconductivity and formation of the QP [20]. Furthermore, back-bending bands can be seen in the binding energy — k_{\parallel} map taken at 10 K [Fig. 2(c)] and its corresponding momentum-integrated EDCs given in Fig. 3(d) where the band bending towards higher binding energy away from the Fermi momentum is marked with a green arc. At low temperatures, the QP is located at the Fermi wave vector where its binding energy is the lowest, but towards the $\bar{\Gamma}$ -point it shows a systematic shift to the higher binding energy. On the other hand, the spectra taken at 180 K exhibits a flat feature at the Fermi level without any signs of band bending [Figs. 3(e) and 3(f)].

The size of the gap and dispersion of the QP are also studied as a function of k_{\parallel} along the red dashed circle is given in the inset of Fig. 2(g). The gap is highly isotropic as a function of k_{\parallel} as subtracted from the EDCs of Fig. 2(g) where the QP peak has the same intensity and location in all directions. This is unlike the nature of the superconducting gap observed in d -wave superconductors and the pseudogap in the CDW phase in which the gap opens in certain parts of the Brillouin zone [18,24]. However, the momentum dependence of the gap observed here is similar to the one expected for s -wave superconductivity [21]. Furthermore, μ -LEED patterns taken at 85 K and 300 K do not exhibit any difference, indicating the absence of structural modulation across the temperature range in which the QP peak, spectral kink, and the Fermi gap form. Therefore, this observation excludes the structural origin of the gap opening such as seen for the CDW phases and shows that these new spectral features are more likely due to the emergence of strongly correlated electrons.

Since the band structure of VSe₂ has been extensively studied, it is surprising to observe such exotic spectral features. Apart from the narrow growth temperature window mentioned above, the HOPG substrate is expected to play a major role in the formation of new spectral features. However, Gr and HOPG are very similar two-dimensional (2D) materials that are not likely to form a strong chemical bond with the VSe₂. Neither substrates are then expected to induce a prominent change in the band structure of the VSe₂ films, especially above the thickness of a few monolayers. Compared to Gr/SiC, cleaved HOPG surfaces can be expected to expose multiple domains, oriented in different directions. These structural differences could indirectly affect the impurities' distribution between the VSe₂ layers, modifying the possible diffusion channels. Therefore, one can speculate on an indirect role of the substrate, inducing relevant modification in the VSe₂ films through minor structural differences.

In summary, we present a detailed ARPES experiment on VSe₂ and show that optimally grown samples host the high-temperature QP, spectral kink, and the Fermi gap which are often signatures for strongly correlated electrons. The size of the gap and the dispersion of the QP as a function of the k_{\parallel} indicate that origin of these new spectral features cannot be simply attributed to the CDW phase. More surprisingly, the similarities between our findings and superconductors are indisputable that the gap shows identical temperature dependence as seen in high- T_c superconductors as an observation of the Fermi gap above the temperature where the QP and spectral kink are suppressed. Hence, our work not only shows the emergence of the novel electronic states in VSe₂, but also opens possibilities to study the spectral features of unconventional superconductors in a different material platform.

This research used the ESM (21-ID-1, 21-ID-2) beamline of the National Synchrotron Light Source II, a U.S. Department of Energy (DOE) Office of Science User Facility operated for the DOE Office of Science by Brookhaven National Laboratory under Contract No. DE-SC0012704. This work also used the resources of the Center for Functional Nanomaterials, Brookhaven National Laboratory, which is supported by the U.S. Department of Energy, Office of Basic Energy Sciences, under Contract No. DE-SC0012704. The initial work on VSe₂ film growth was supported by the University of Connecticut under the UCONN-REP (Grant No. 4626510).

[1] S. Manzeli, D. Ovchinnikov, D. Pasquier, O. V. Yazyev, and A. Kis, 2D transition metal dichalcogenides, *Nat. Rev. Mater.* **2**, 17033 (2017).
 [2] F. Clerc, C. Battaglia, M. Bovet, L. Despont, C. Monney, H. Cercellier, M. G. Garnier, P. Aebi, H. Berger, and L. Forró, Lattice-distortion-enhanced electron-phonon coupling and Fermi surface nesting in 1T-TaS₂, *Phys. Rev. B* **74**, 155114 (2006).
 [3] Y. D. Wang, W. L. Yao, Z. M. Xin, T. T. Han, Z. G. Wang, L. Chen, C. Cai, Y. Li, and Y. Zhang, Band insulator to Mott insulator transition in 1T-TaS₂, *Nat. Commun.* **11**, 4215 (2020).

[4] Y. Fang, J. Pan, D. Zhang, D. Wang, H. T. Hirose, T. Terashima, S. Uji, Y. Yuan, W. Li, Z. Tian *et al.*, Discovery of superconductivity in 2M WS₂ with possible topological surface states, *Adv. Mater.* **31**, 1901942 (2019).
 [5] E. Morosan, H. W. Zandbergen, B. Dennis, J. Bos, Y. Onose, T. Klimczuk, A. Ramirez, N. Ong, and R. J. Cava, Superconductivity in Cu_xTiSe₂, *Nat. Phys.* **2**, 544 (2006).
 [6] J. M. Riley, W. Meevasana, L. Bawden, M. Asakawa, T. Takayama, T. Eknapakul, T. Kim, M. Hoesch, S.-K. Mo, H. Takagi *et al.*, Negative electronic compressibility and tunable spin splitting in WSe₂, *Nat. Nanotechnol.* **10**, 1043 (2015).

- [7] P. Chen, W. W. Pai, Y.-H. Chan, V. Madhavan, M.-Y. Chou, S.-K. Mo, A.-V. Fedorov, and T.-C. Chiang, Unique Gap Structure and Symmetry of the Charge Density Wave in Single-Layer VSe₂, *Phys. Rev. Lett.* **121**, 196402 (2018).
- [8] P. M. Coelho, K. Nguyen Cong, M. Bonilla, S. Kolekar, M.-H. Phan, J. Avila, M. C. Asensio, I. I. Oleynik, and M. Batzill, Charge density wave state suppresses ferromagnetic ordering in VSe₂ monolayers, *J. Phys. Chem. C* **123**, 14089 (2019).
- [9] P. K. J. Wong, W. Zhang, F. Bussolotti, X. Yin, T. S. Heng, L. Zhang, Y. L. Huang, G. Vinai, S. Krishnamurthi, D. W. Bukhvalov *et al.*, Evidence of spin frustration in a vanadium diselenide monolayer magnet, *Adv. Mater.* **31**, 1901185 (2019).
- [10] G. Duvjir, B. K. Choi, I. Jang, S. Ulstrup, S. Kang, T. Thi Ly, S. Kim, Y. H. Choi, C. Jozwiak, A. Bostwick *et al.*, Emergence of a metal-insulator transition and high-temperature charge-density waves in VSe₂ at the monolayer limit, *Nano Lett.* **18**, 5432 (2018).
- [11] J. G. Si, W. J. Lu, H. Y. Wu, H. Y. Lv, X. Liang, Q. J. Li, and Y. P. Sun, Origin of the multiple charge density wave order in 1T-VSe₂, *Phys. Rev. B* **101**, 235405 (2020).
- [12] V. N. Strocov, M. Shi, M. Kobayashi, C. Monney, X. Wang, J. Krempasky, T. Schmitt, L. Patthey, H. Berger, and P. Blaha, Three-Dimensional Electron Realm in VSe₂ by Soft-x-Ray Photoelectron Spectroscopy: Origin of Charge-Density Waves, *Phys. Rev. Lett.* **109**, 086401 (2012).
- [13] S. Barua, M. C. Hatnean, M. Lees, and G. Balakrishnan, Signatures of the kondo effect in VSe₂, *Sci. Rep.* **7**, 10964 (2017).
- [14] W. Yu, J. Li, T. S. Heng, Z. Wang, X. Zhao, X. Chi, W. Fu, I. Abdelwahab, J. Zhou, J. Dan *et al.*, Chemically exfoliated VSe₂ monolayers with room-temperature ferromagnetism, *Adv. Mater.* **31**, 1903779 (2019).
- [15] S. Sahoo, U. Dutta, L. Harnagea, A. K. Sood, and S. Karmakar, Pressure-induced suppression of charge density wave and emergence of superconductivity in 1T - VSe₂, *Phys. Rev. B* **101**, 014514 (2020).
- [16] N. Mannella, W. L. Yang, X. J. Zhou, H. Zheng, J. F. Mitchell, J. Zaanen, T. P. Devereaux, N. Nagaosa, Z. Hussain, and Z.-X. Shen, Nodal quasiparticle in pseudogapped colossal magnetoresistive manganites, *Nature (London)* **438**, 474 (2005).
- [17] H. Ding, J. R. Engelbrecht, Z. Wang, J. C. Campuzano, S.-C. Wang, H. B. Yang, R. Rogan, T. Takahashi, K. Kadowaki, and D. G. Hinks, Coherent Quasiparticle Weight and Its Connection to High-T_c Superconductivity from Angle-Resolved Photoemission, *Phys. Rev. Lett.* **87**, 227001 (2001).
- [18] I. K. Drozdov, I. Pletikosić, C.-K. Kim, K. Fujita, G. Gu, J. Davis, P. Johnson, I. Božović, and T. Valla, Phase diagram of Bi₂Sr₂CaCu₂O_{8+δ} revisited, *Nat. Commun.* **9**, 5210 (2018).
- [19] H. Matsui, T. Sato, T. Takahashi, S.-C. Wang, H.-B. Yang, H. Ding, T. Fujii, T. Watanabe, and A. Matsuda, BCS-Like Bogoliubov Quasiparticles in High-T_c Superconductors Observed by Angle-Resolved Photoemission Spectroscopy, *Phys. Rev. Lett.* **90**, 217002 (2003).
- [20] T. Kondo, Y. Hamaya, A. D. Palczewski, T. Takeuchi, J. Wen, Z. Xu, G. Gu, J. Schmalian, and A. Kaminski, Disentangling cooper-pair formation above the transition temperature from the pseudogap state in the cuprates, *Nat. Phys.* **7**, 21 (2011).
- [21] K. Nakayama, T. Sato, P. Richard, T. Kawahara, Y. Sekiba, T. Qian, G. F. Chen, J. L. Luo, N. L. Wang, H. Ding, and T. Takahashi, Angle-Resolved Photoemission Spectroscopy of the Iron-Chalcogenide Superconductor Fe_{1.03}Te_{0.7}Se_{0.3}: Strong Coupling Behavior and the Universality of Interband Scattering, *Phys. Rev. Lett.* **105**, 197001 (2010).
- [22] P. Richard, T. Qian, and H. Ding, ARPES measurements of the superconducting gap of Fe-based superconductors and their implications to the pairing mechanism, *J. Phys.: Condens. Matter* **27**, 293203 (2015).
- [23] U. Chatterjee, J. Zhao, M. Iavarone, R. Di Capua, J. Castellan, G. Karapetrov, C. Malliakas, M. G. Kanatzidis, H. Claus, J. Ruff *et al.*, Emergence of coherence in the charge-density wave state of 2H-NbSe₂, *Nat. Commun.* **6**, 6313 (2015).
- [24] G. Grüner, The dynamics of spin-density waves, *Rev. Mod. Phys.* **66**, 1 (1994).